Supporting Information for

Accelerating evaluation of the mobility of ionic liquids modulated PEDOT flexible electronics using machine learning

Wei-Lu Ding,[a] Yumiao Lu,[a] Xing-Liang Peng,[b] Hao Dong,[a] Wei-Jie Chi,[c] Xiaoqing Yuan,[a] Zhu-Zhu Sun*[d] and Hongyan He*[a,e,f]

[a] *Beijing Key Laboratory of Ionic Liquids Clean Process, CAS Key Laboratory of Green Process and Engineering, State Key Laboratory of Multiphase Complex Systems, Institute of Process Engineering, Chinese Academy of Sciences, Beijing 100190, China*

[b] *MOE Key Laboratory of Organic OptoElectronics and Molecular Engineering, Department of Chemistry, Tsinghua University, Beijing 100084, China*

[c] *Singapore Science and Math Cluster, Singapore University of Technology and Design, Singapore 487372, Singapore*

[d] *College of Physics and Electronic Engineering, Heze University, Heze 274015, China*

[e] *Innovation Academy for Green Manufacture Chinese Academy of Sciences, Beijing 100190, China*

[f] *Dalian National Laboratory for Clean Energy, Dalian 116023, China*

Corresponding Author:

Email: sunzhuzhu@hezeu.edu.cn; hyhe@ipe.ac.cn

Contents

The model construction of IL-PEDOT:Tos

The ionic liquid (IL) modulated PEDOT:Tos hydrogels with low and high concentration (L-PEDOT:Tos and H-PEDOT:Tos) as well as real experimental ratio were constructed by adding different quantities of each species. Generally, PEDOT is commonly constituted by 3 ~ 18 repeated monomer units (EDOT)[1], therefore, we selected oligomeric PEDOT containing 9 EDOT units in balance of computational accuracy and time-consuming. Based on the experimental report, an oxidation level of 33.3% doping (charge equals to +3) of PEDOT was detected. Hence, for (1) L-PEDOT:Tos system, 12 PEDOT, 36 Tos (-1 charged), and 5356 water were added in a sufficient large 9 × 6 × 4 nm^3 unit cell based on our previous work; (2) H-PEDOT:Tos system, 28 PEDOT, 84 Tos, and 2670 water were added in same box size. After the pre-balancing, 96 cation-anion pairs were introduced on top of the box to permit them diffusion into the pristine L/H-PEDOT:Tos solution. The amorphous solution model was generated by Packmol code[2] as the start point to perform molecular dynamic (MD) simulations implemented in LAMMPS code[3]. The parameters of bonded and van der Waals (vdW) nonbonded were taken from OPLS-AA force field[4], the water solvent was described by SPC/E model[5], and atomic charge used for Coulombic nonbonded was obtained by the restrained electrostatic potential (RESP) method[6] which was implemented by Multiwfn code[7] on top of the structure optimized by B3LYP/6-311G(d,p) level via Gaussian 09 program[8]. Each system was firstly relaxed via conjugate gradient algorithm, then followed by 5 ns NPT run (293 K, 1 bar) using the Parrinello-Rahman barostat, subsequent by equilibration in the NVT ensemble (293 K, 1 bar) using the Nose-Hoover thermostat until the density and total energy reached equilibrium (~ 20 ns). The time step in whole simulations was 0.1 fs, and cutoff for the vdW interaction was 12 Å. Finally, a 10 ns production run for the radial distribution function (RDF) simulations and sampling were performed. 5000 snapshots for hole transport simulations by quantum mechanics calculations were abstracted every 10 ps.

To obtain the hole hopping rate (k_n) and mobility (μ), the critical items of transfer integral (V_{ij}), reorganization energy (λ), and hopping site energy (the HOMO energy) were computed separately in different level by Gaussian program. The V_{ij} was performed by semiempirical ZINDO/S[9-10] level for dimeric fragments, and the λ was

finished by B3LYP/6-311G(d,p) to perform the structure optimization and frequency calculation.

The calculation of reorganization energy

The reorganization energy (λ) is related to the energy change with the geometry relaxation during charge transport, which can be evaluated by the adiabatic potential energy surface method (the four-point method) and normal mode analysis. The former is expressed as[11]:

$$\lambda = \lambda_1 + \lambda_2 = (E_+^0 - E_0) + (E_0^+ - E_+^+)$$

where E_+^0 is the energy of the neutral molecule calculated on top of the optimized cationic state, E_0 is the energy of the optimized neutral molecule at ground state, E_0^+ is the energy of the cation calculated on top of the optimized neutral state, and E_+^+ is the energy of the optimized cation, respectively.

And the normal mode analysis assigns the λ to the contribution from each vibrational mode:[12]

$$\lambda = \lambda_1 + \lambda_2 = \sum_i \lambda_{1i} + \sum_j \lambda_{2j} = \sum_i \frac{1}{2}\omega_i \Delta Q_i^2 + \sum_j \frac{1}{2}\omega_j \Delta Q_j^2$$

where λ_{1i} and λ_{2j} stand for the contributions to the λ from vibrational modes i and j of the neutral and cationic geometries separately, ω_i and ω_j represent for the vibrational frequencies of modes i and j, and ΔQ_i and ΔQ_j are the displacements along the ith and jth mode coordinates between the equilibrium positions of neutral and cationic states, respectively. By contrast to the V_{ij}, a minimized λ potentially ensures a large hole hopping rate k_n. And in this work, we used the first method to calculate λ, and its value is 0.1 eV.

The calculation of hole mobility

The hole mobility (μ) can be obtained based on the non-adiabatic Marcus charge transfer theory[13-15]:

$$k_n = \frac{2\pi}{\hbar}\left|V_{ij}\right|^2 \sqrt{\frac{1}{4\pi k_{\mathrm{B}}\mathrm{T}\lambda}} \exp\left[-\frac{(\Delta G_{ij}+\lambda)^2}{4\lambda k_{\mathrm{B}}\mathrm{T}}\right]$$

where $\hbar$ is reduced Planck's constant, V_{ij} is the transfer integral, k_{B} is Boltzmann's constant, T is temperature in Kelvin, λ is the reorganization energy, and ΔG_{ij} is the energy difference in sites i and j, respectively. Accordingly, the hole mobility (μ) is estimated by Einstein equation:[16]

$$\mu = \frac{eD}{k_{\mathrm{B}}\mathrm{T}}$$

$$D = \frac{1}{2d}\sum_n r_n^2 k_n p_n$$

where e and D in numerator represent for the unit charge and diffusion coefficient. Correspondingly, to calculate D, a spatial dimensionality d should be defined (here taken as 1 for amorphous morphology), and associated centroid to centroid distance (r_n), k_n, as well as the hopping probability for the nth hopping pathway ($p_n = k_n / \sum_n k_n$) should be as the input to obtain the diffusion coefficient.

Experiment

Materials

PEDOT:PSS aqueous solution (1.5% in water) was supplied by Shanghai Aladdin Biochemical Technology Co. LTD. High purity [EMIM][TFSI] (99.0%) were purchased from Shanghai Chengjie Chemical Co. LTD. The chemicals were used as received without any treatment.

Sample preparation

[EMIM][TFSI] was dissolved in ultra-pure water at the concentration of 1×10^{-3} mol L^{-1} and was subsequently sonicated for 10 minutes. PEDOT:PSS was added to the diluted IL solution at the molar ratio of PEDOT:PSS:H_2O at 1:440 and 1:880 and vigorously stirred at room temperature overnight. To prepare the films, the mixture solutions were spin-casted onto ITO substrates that have been cleaned with a detergent solution: sonicated in deionized water, acetone, and isopropyl alcohol for 10 min each and then dried at 130 °C for 15 min. The volume of spin coating solution varies from 1 μL, 2 μL, 5 μL, to 10 μL. To obtain the stable surface structure, the sample was left in air for at least 5 hours before AFM scanning.

Characterization

The morphological feature of the sample was characterized by Multimode Nanoscope 8 AFM (Bruker, USA) at room temperature. AFM tips (SNL-10, A tip) with spring constant of ~ 0.2 N/m and radius of ~ 2 nm were used. For each sample, 3 different areas at least were scanned to ensure the repeatability of the data. The conductivity measurement was performed by METTLER TOLEDO FE30.

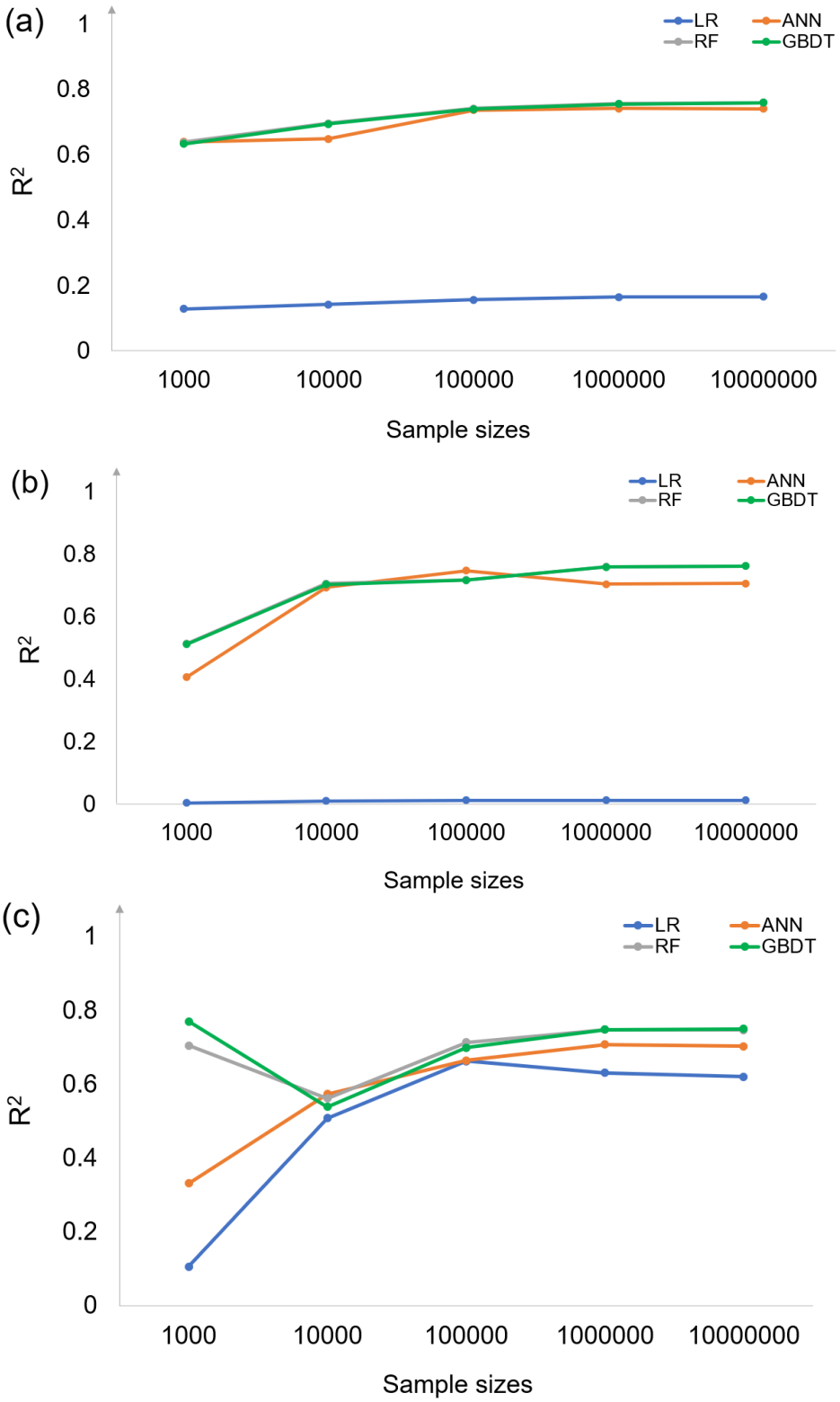

Fig. S1. The R^2 varies with the variation of sample size trained by different algorithms. a Geometric feature as descriptors. **b** Electronic feature as descriptors (the decision trees used in RF and GBDT algorithms are 350). and **c** Coulomb matrix (CM) as descriptor.

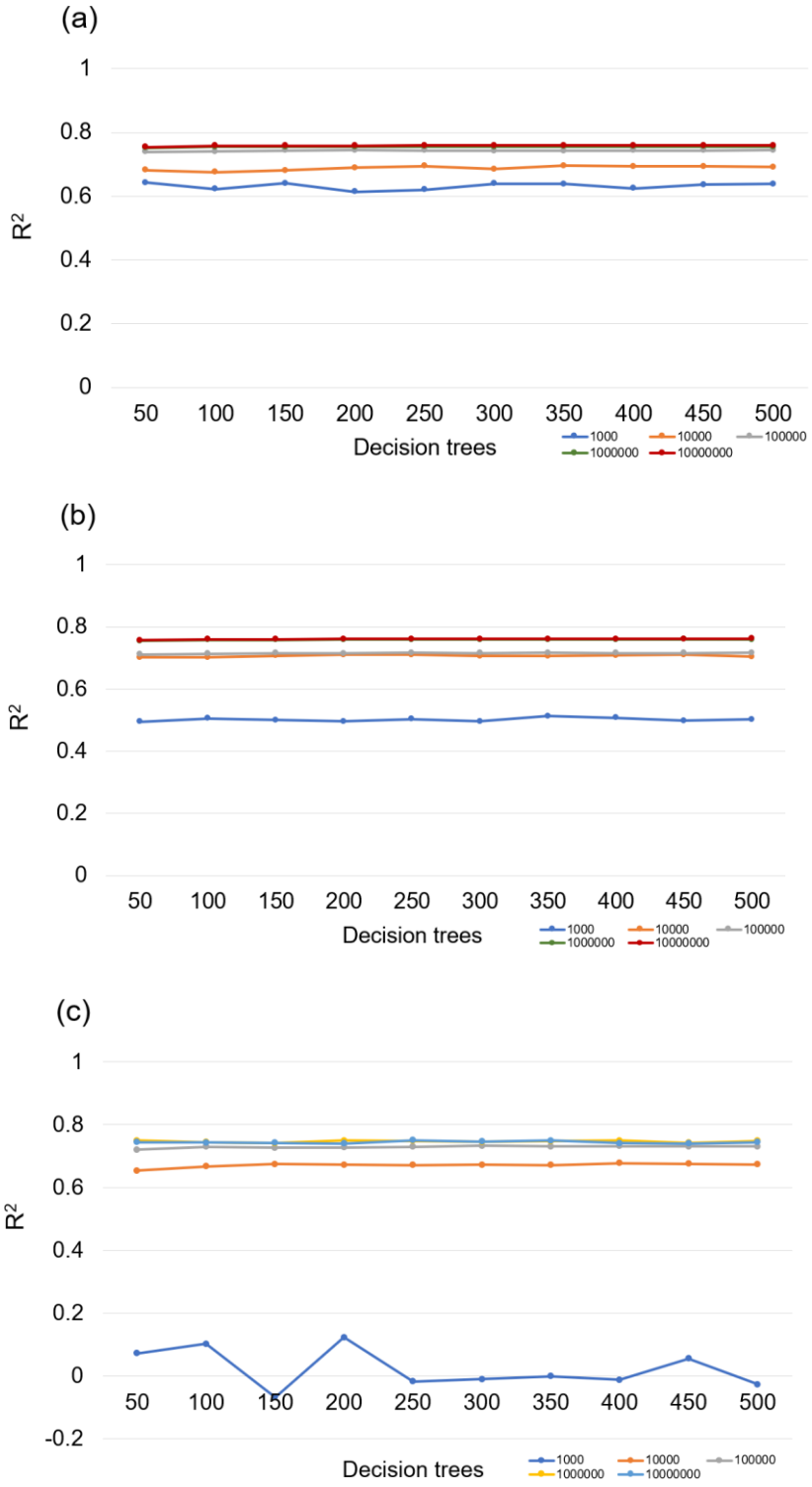

Fig. S2. The R^2 varies with the variation of sample size and decision trees trained by RF algorithm. **a** Geometric features as descriptor. **b** Electronic features as descriptor. and **c** Coulomb matrix (CM) as descriptor (The GBDT algorithm produces almost identical results, has not shown).

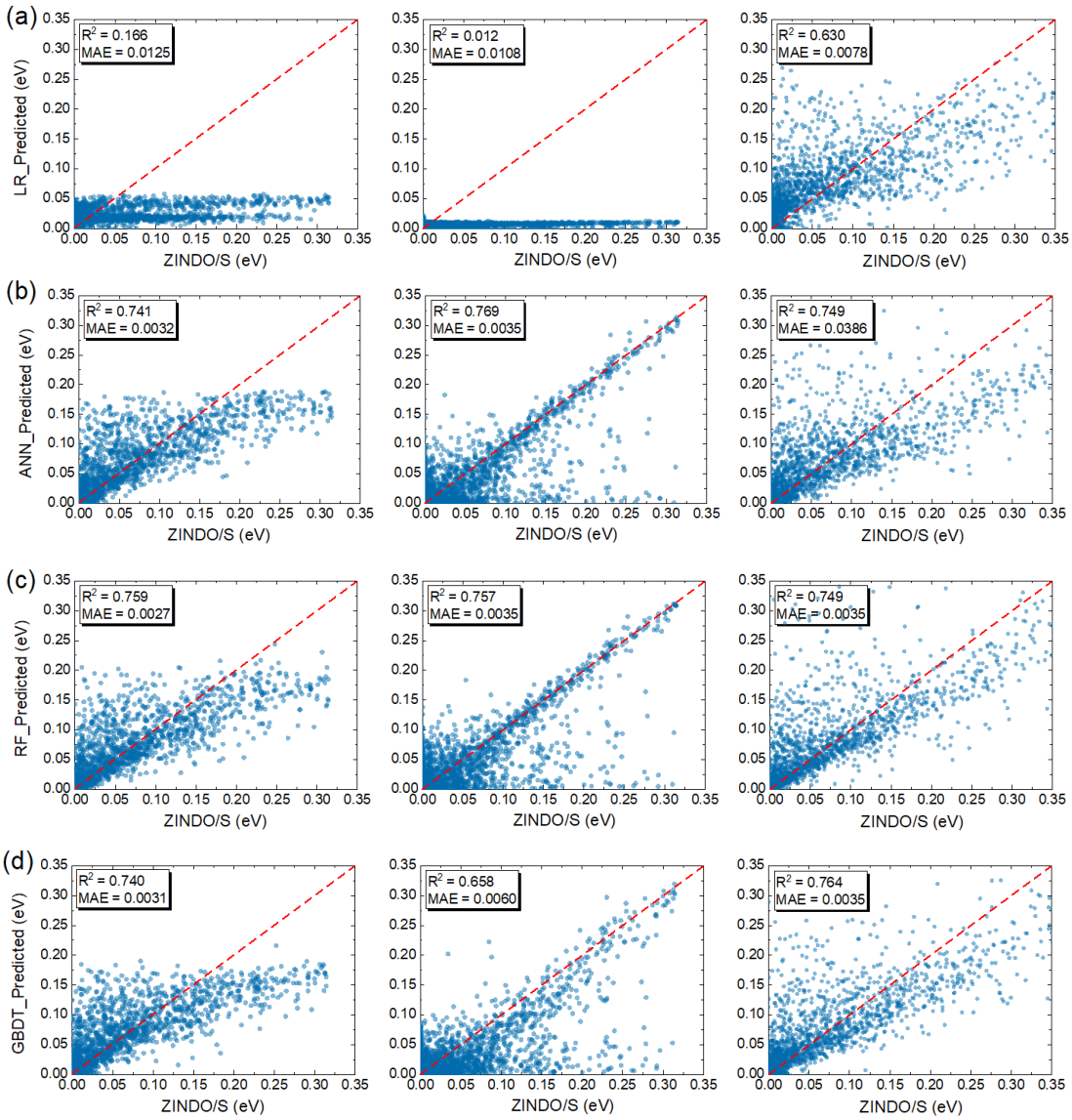

Fig. S3. **The predicted $|V_{ij}|$ for [EMIM]Cl-L-PEDOT:Tos system.** Parity plot between the ZINDO/S calculated and different ML learner predicted $|V_{ij}|$ from 10-fold cross-validation for **a** LR, **b** ANN, **c** RF, and **d** GBDT algorithm (the left, middle, and right are the results based on geometric feature, electronic feature, and C_{ij} feature as descriptors, and the unit of MAE value is in eV).

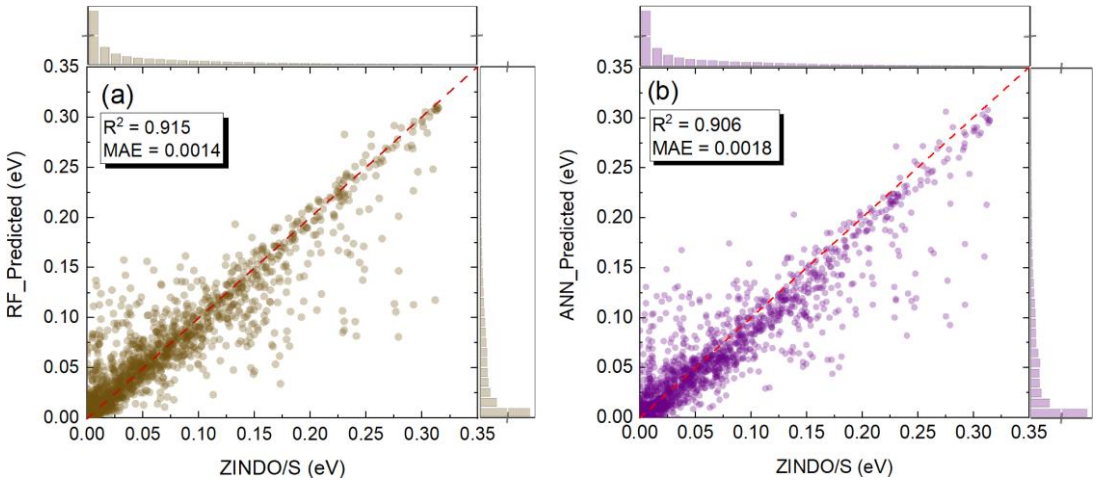

Fig. S4. The predicted $|V_{ij}|$ for [EMIM]Cl-L-PEDOT:Tos system by using combined geometric and electronic features. Parity plot between the ZINDO/S calculated and ML learner predicted $|V_{ij}|$ from 10 fold cross-validation have been shown for **a** by RF with 300 decision trees and **b** by ANN with 6 hidden layers (the numbers of neurons in each layer are100, and the unit of MAE value is in eV).

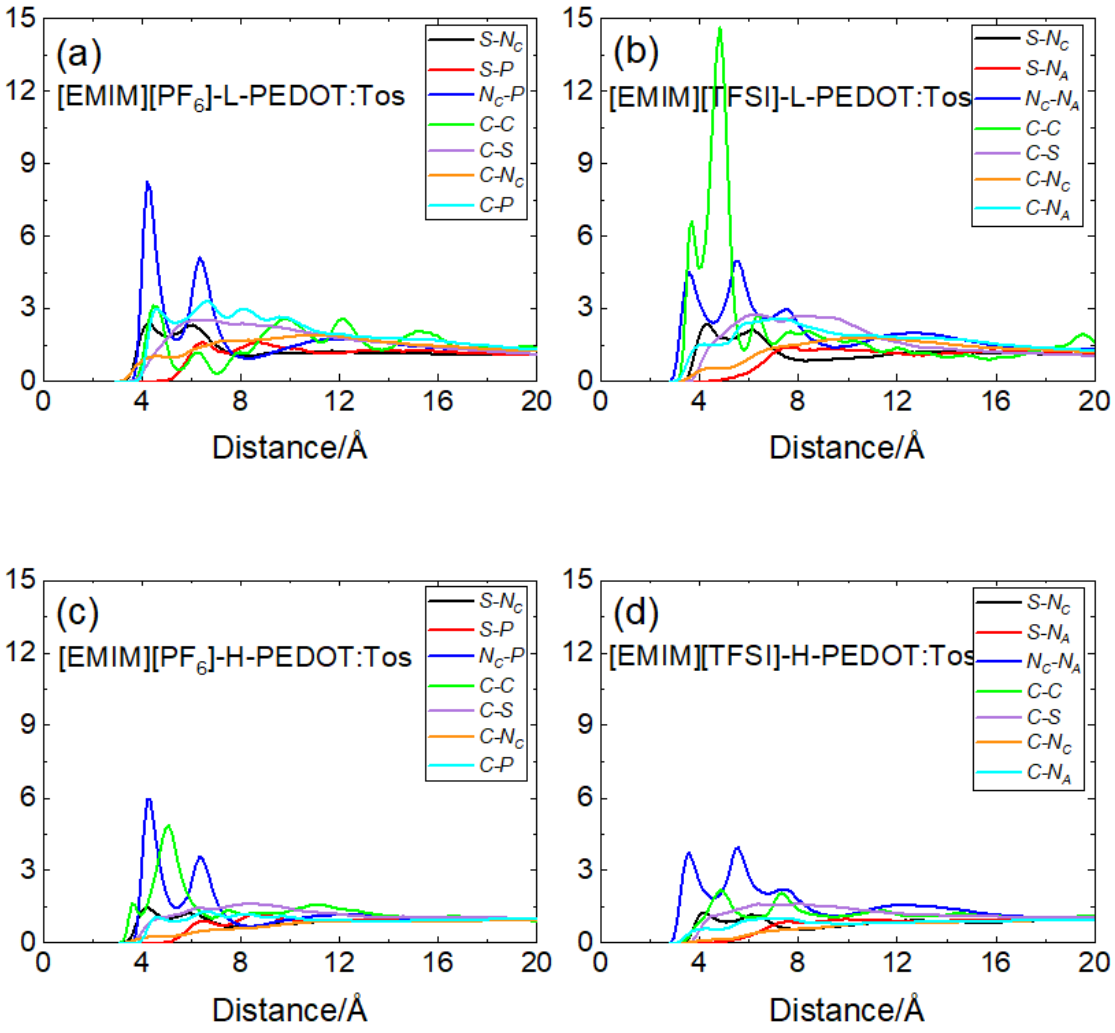

Fig. S5. The radial distribution function (RDF) of ILs modulated PEDOT:Tos. a and **c** [EMIM][PF_6] modulated L-PEDOT:Tos and H-PEDOT:Tos solution. **b** and **d** [EMIM][TFSI] modulated L-PEDOT:Tos and H-PEDOT:Tos solution, respectively.

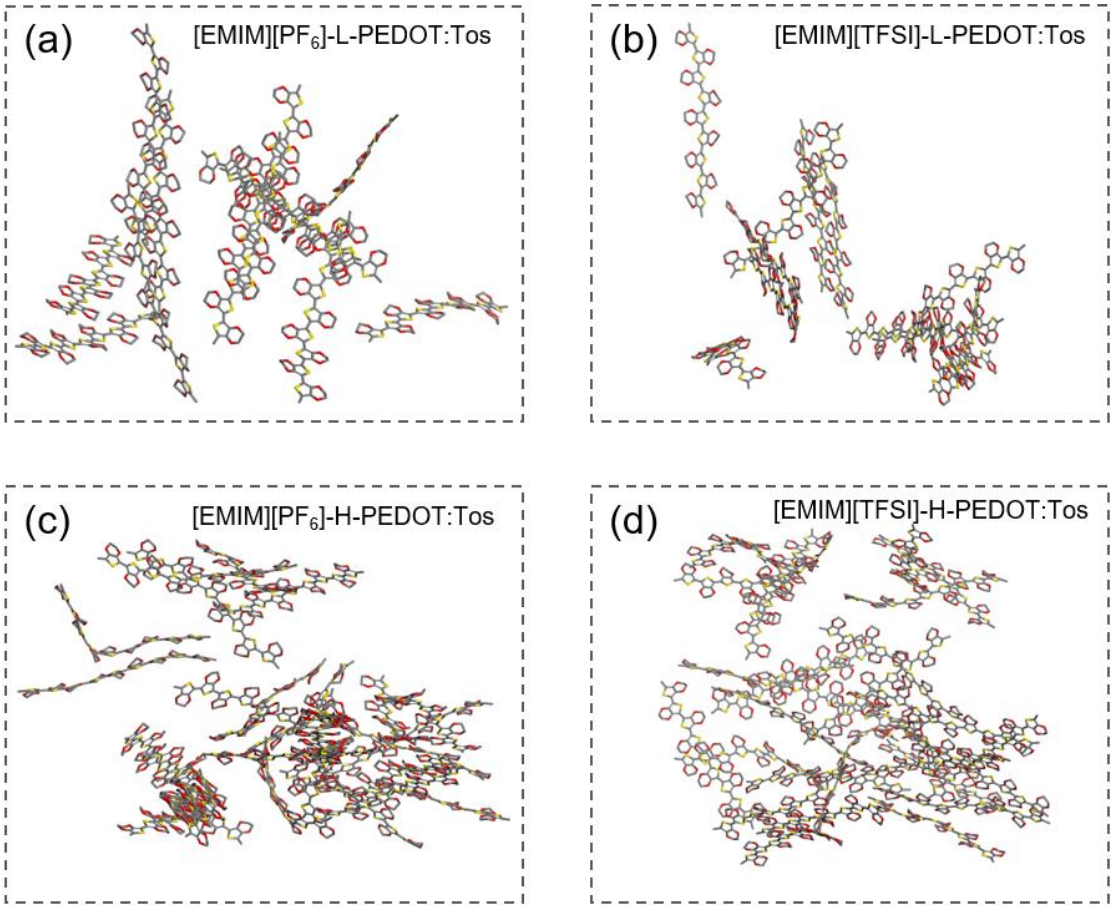

Fig. S6. The stacked PEDOT abstracted from the last MD snapshot. a and **c** [EMIM][PF_6] modulated L-PEDOT:Tos and H-PEDOT:Tos solution. **b** and **d** [EMIM][TFSI] modulated L-PEDOT:Tos and H-PEDOT:Tos solution, respectively.

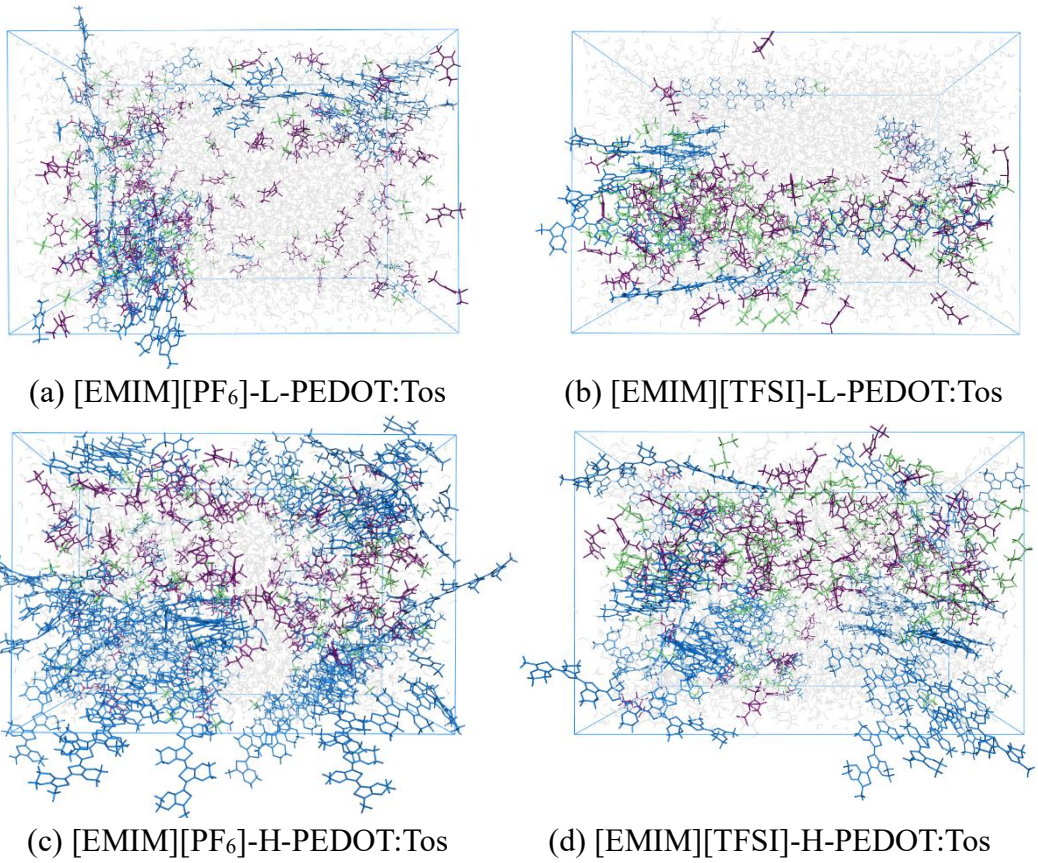

(a) [EMIM][PF_6]-L-PEDOT:Tos (b) [EMIM][TFSI]-L-PEDOT:Tos

(c) [EMIM][PF_6]-H-PEDOT:Tos (d) [EMIM][TFSI]-H-PEDOT:Tos

Fig. S7. The last MD snapshots for IL decorated PEDOT:Tos solution. **a** and **c** [EMIM][PF_6] modulated L-PEDOT:Tos and H-PEDOT:Tos solution. **b** and **d** [EMIM][TFSI] modulated L-PEDOT:Tos and H-PEDOT:Tos solution, respectively.

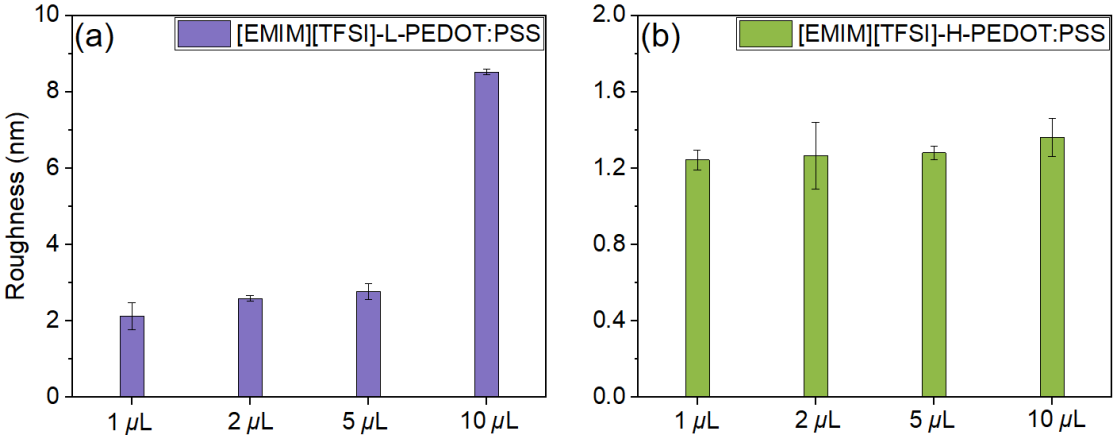

Fig. S8. The roughness for [EMIM][TFSI] decorated PEDOT:PSS aqueous. **a** The sample of L-PEDOT:PSS. **b** The sample of H-PEDOT:PSS.

References

1. K. Nara, I. Petsagkourakis, S. Chen, M. Berggren, X. Crispin, M. P. Jonsson, I. Zozoulenko, Electric transport properties in PEDOT thin films, Conjugated polymers, CRC Press, (2019), 45-128.
2. L., Martinez, R. Andrade, E. G. Birgin, J. M. Martinez, Packmol: a package for building initial configurations for molecular dynamics simulations. J. Comput. Chem., 30, (2009), 2157-2164.
3. S. Plimpton, Fast parallel algorithms for short-range molecular-dynamics. J. Comput. Phys., 117, (1995), 1-19.
4. W. L. Jorgensen, D. S. Maxwell, J. TiradoRives, Development and testing of the opls all-atom force field on conformational energetics and properties of organic liquids. J. Am. Chem. Soc., 118, (1996), 11225-11236.
5. P. Mark, L. Nilsson, Structure and dynamics of the TIP3P, SPC, and SPC/E water models at 298 K. J. Phy. Chem. A, 105, (2001), 9954-9960.
6. J. Zeng, L. Duan, J. Z. Zhang, Y. Mei, A numerically stable restrained electrostatic potential charge fitting method, J. Comput. Phys., 34, (2013), 847-853.
7. T. Lu, F. Chen, Multiwfn: a multifunctional wavefunction analyzer, J. Comput. Phys., 33, (2012), 580-592.
8. Frisch, M. J.; Trucks, G. W.; Schlegel, H. B.; Scuseria, G. E.; Robb, M. A.; Cheeseman, J. R.; Zakrzewski, V. G.; Montgomery, J. A.; Stratmann, R. E.; Burant, J. C. et al. Gaussian 09, revision D.01; Gaussian, Inc.: Wallingford, CT, 2013.
9. J. Ridley, M. Zerner, An Intermediate neglect of differential overlap technique for spectroscopy: pyrrole and the azines, Theor. Chim. Acta., 32, (1973), 111-134.
10. E. D. Miller, M. L. Jones, M. M. Henry, B. Stanfill, E. Jankowski, Machine learning predictions of electronic couplings for charge transport calculations of P3HT, AIChE J., 65, (2019), e16760.
11. M. N. Paddon-Row, Orbital interactions and long-range electron transfer, Adv. Phys. Org. Chem., 38, (2003), 1.
12. Z. Shuai, L. Wang, C. Song, Theory of charge transport in carbon electronic materials. Springer Science & Business Media, (2012).
13. R. A. Marcus, S. Norman, Electron transfers in chemistry and biology, BBA-Bioenergetics, 811 (1985) 265-322.
14. R. A. Marcus, Electron transfer reactions in chemistry, theory and experiment, Rev. Mod. Phys. 65 (1993) 599.
15. R. A. Marcus, On the theory of electron-transfer reactions. vi. unified treatment for homogeneous and electrode reactions, J. Chem. Phys., 43 (1965) 679-701.
16. L. B. Schein, A. R. McGhie, Band-hopping mobility transition in naphthalene and deuterated naphthalene, Phys. Rev. B: Condens. Matter Mater. Phys. 20 (1979) 1631-1639.